Table 1. Data collection and structure refinement statistics

Parameters	WT PvDHFR–Pyr	WT PvDHFR–Pyr20	SP21–Pyr	SP21–Pyr20
Space group	C2	C2	C2	C2
Unit cell *a*, *b*, and *c*, Å; and β, °	134.28, 55.74, 45.72, 107.09	130.48, 55.57, 45.27, 106.76	135.27, 54.40, 46.09, 108.13	132.00, 56.31, 45.67, 107.50
Resolution, Å	20–1.90	20–3.00	20–2.50	20–2.25
Completeness, % (final shell, %)	99.1 (99.1)	99.7 (99.9)	98.9 (99.7)	97.5 (97.5)
Unique reflections	24,153	6,307	11,042	14,912
Redundancy	3.21	3.40	4.85	3.72
R_{sym}, % (final shell)*	4.4 (40.6)	7.9 (31.5)	9.2 (37.9)	4.5 (30.4)
$\langle I/\sigma \rangle$ (final shell)	14.8 (3.3)	11.5 (3.8)	10.1 (3.8)	11.8 (2.0)
R factor/R_{free},† %	20.79/25.82	19.08/29.99	19.39/28.18	21.33/27.60
Average *B* factor, Å^2	53.5	41.63	49.69	63.80
No. of atoms	2,094	1,907	2,005	2,031
Nonhydrogen protein	1763	1781	1769	1760
Ligands	65	77	76	76
Solvents	266	147	62	195
rms deviation				
Bond lengths, Å	0.0073	0.0096	0.0091	0.0079
Bond angles, °	1.187	1.204	1.190	1.160

*$R_{sym} = \Sigma|I - \langle I \rangle|/\Sigma I$, where *I* is the observed intensity and $\langle I \rangle$ is the average intensity from multiple observations of symmetry-related reflections.
†*R* factor $= \Sigma_{hkl}|F_o(hkl) - F_c(hkl)|/\Sigma_{hkl} F_o(hkl)$, where $F_o(hkl)$ and $F_c(hkl)$ are the observed and calculated structure factor amplitudes for reflection *hkl*. R_{free} is computed by using randomly selected 5% of the data that were excluded throughout refinement.

with Pyr20 (K_i = 1.55 nM) were prepared by ligand-exchange soaking of the WT PvDHFR–Pyr complex crystals in a stabilizing solution containing 3 mM Pyr20 for 2–3 days at 4°C. Complexes of SP21 PvDHFR with 1 mM Pyr or Pyr20 were cocrystallized in 100 mM Mes at pH 6.0. Before flash-cooling, the crystals were transferred into a reservoir solution supplemented with 20% glycerol and immediately frozen in the cryostream. All diffraction data sets were measured at 120 K on a generator (Rigaku, Tokyo) with an R-AXIS IV++ detector. All data were integrated and scaled by using D*TREK (22). Data processing and refinement statistics are given in Table 1.

Structure Determination and Refinement. The structure of PvDHFR–NADPH–Pyr ternary complex was determined by using the molecular replacement method using the structure of the N-terminal DHFR domain of PfDHFR-TS [Protein Data Bank ID code 1J3J] as a search model with the program CCP4-AMORE (23). Electron density maps were inspected and models were manually built by using the graphics program XTALVIEW (24). The refinement was carried out by using CNS (25) and included individual *B* factor refinement, simulated annealing, and positional refinement using the parameters of Engh and Huber (26). The other three PvDHFR complex structures were solved with difference Fourier technique or with molecular replacement by using the structural model of the WT PvDHFR–NADPH–Pyr complex and refined with CNS. Water molecules were inserted automatically and inspected manually. The model displays good stereochemistry with no disallowed φ/ψ angles for all of the final models (Table 1), as verified by PROCHECK (27). Structural alignments were performed by CCP4-TOPS (28), and figures were prepared with PYMOL (www.pymol.org).

Kinetic Studies. Inhibition experiments were performed as described in ref. 10, and the inhibition constants (K_i) were calculated from a nonlinear least-square equation for competitive inhibitor by using KALEIDAGRAPH 3.5 (Synergy Software, Reading, PA).

Results and Discussion

Overall Structure of *P. vivax* DHFR. The crystal structure of 238-residue N-terminal DHFR domain of the bifunctional PvDHFR-TS enzyme shows that PvDHFR is a monomer of $\approx 38 \times 49 \times 62$ Å, whereas the full-length PfDHFR-TS exists as a homodimeric enzyme with extensive intersubunit contacts between the two TS domains. The PvDHFR domain, consisting of an eight-stranded mixed β-sheet ($\beta_{A\text{-}H}$) flanked by four α-helices ($\alpha_{B,C,E,F}$) (Fig. 1*A*), shares a similar overall polypeptide fold to that characteristic of other DHFRs (29) with two additional short α-helices (α_A and α_D). Similarity can be noted in the overall folding with that previously modeled structure (30), although there are many significant differences, particularly in the insert regions. The DHFR domains of *P. vivax* and *P. falciparum* share 66% sequence identity, and their structures can be superimposed well with a rms deviation (rmsd) of 0.87 Å for 194 C^α atoms (Fig. 1*B*). Plasmodial DHFRs has two unique regions of insert sequences (in *P. vivax*; Insert-1, residues 19–35, and Insert-2, residues 63–107). In our PvDHFR structure, Insert-1 adopted a flexible loop connecting between β_A and α_B, with a different orientation from that of PfDHFR-TS structure by as much as 13–15 Å for residues 25–28 (Fig. 1*B*). Because the Insert-1 of PfDHFR has been shown to interact with the TS domain, the difference in the insert arrangement may be due to the lack of the intact TS domain in the PvDHFR structures presented or may indicate the presence of different interactions in the enzymes from the two species. Although crystals of PvDHFR-TS had been obtained, they gave diffraction quality with insufficient resolution to yield the structure of the bifunctional enzyme for direct comparison with PfDHFR-TS (P.K., unpublished results). Similar to that of PfDHFR, although distinct from the homology model, Insert-2 formed another α-helical stretch α_{i2} (residues 66–84). Conserved basic residues in the middle of α_{i2}, pointing toward the interior of the protein, make extensive contacts with the globular structure and hence stabilize its orientation. Although Lys-75 forms polar contacts with the main-chain C=O of Asp-6 and the carboxylate side chain of Asp-9, Arg-76 extensively interacts with the carboxylate group of Asp-9, main-chain carbonyl oxygen atoms of Val-7, Tyr-167, and Tyr-168. At the C terminus of α_{i2}, the side chain of Glu-83 interacts with the amine group of the Lys-164. No electron density for residues 85–105 in the Insert-2, probably due to protein flexibility, was visible, and thus these residues were

BIOCHEMISTRY

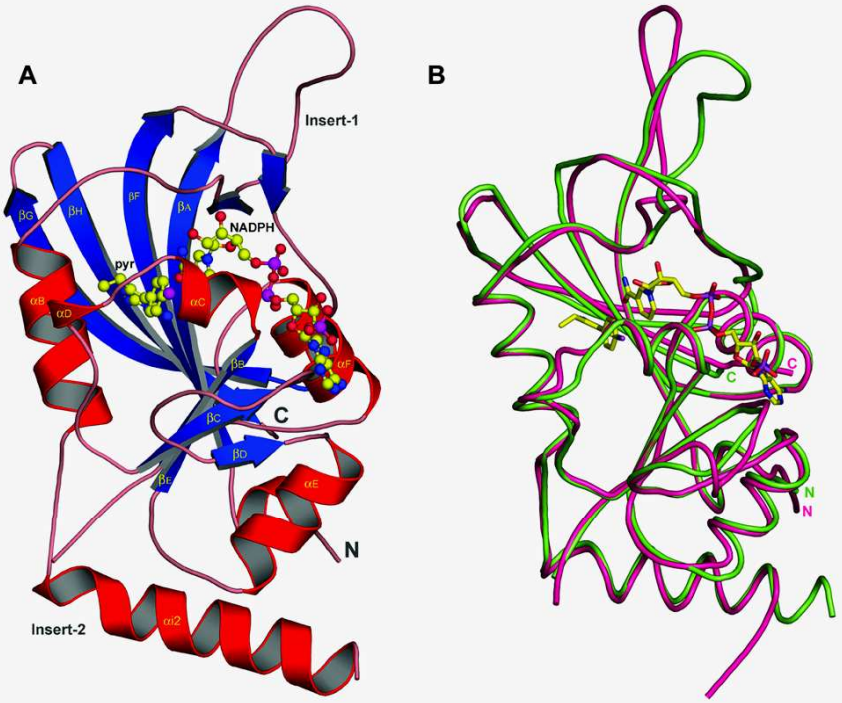

Fig. 1. C ital structure of the DHFR domain of *P. vivax*. (*A*) Structure of *P. vivax* DHFR complexed with NADPH and Pyr; α-helices are in red, and β-strands are in blue, in iding the Insert-1 loop and the Insert-2 α-helix. The carbons, nitrogen, oxygen, and chlorine atoms of Pyr and NADPH are shown in yellow, blue, red, and mage a, respectively. (*B*) Comparison of the DHFR domains from *P. vivax* (green) and *P. falciparum* (magenta). The superimposed structures demonstrate overall sti tural similarity with major deviation in the insert regions.

not inc led in the model. The flexible conformation was revealed by relatively higher *B* factor toward the visible region of Insert-2, of which conserved residues comprise several basic residues, suggesting a possible mRNA binding site and translational regulation of the protein (31).

Pyr Binding with the Active Site. Pyr binds at the active site of PvDHFR with its pyrimidine ring buried in the interior of the deep cleft through hydrogen bonds (H-bonds) and van der Waals interactions (Fig. 2*A*). H-bonds play a significant role in the binding of the Pyr; N1 and 2-amino nitrogen atoms of Pyr are H-bonded to the carboxylate oxygen atoms of Asp-53 (distances of 2.57 and 2.89 Å, respectively), and the 4-amino nitrogen atom is H-bonded to the main-chain carbonyl oxygen atoms of Ile-13 and Ile-173 (distances of 2.96 and 2.92 Å, respectively). In addition, the N2 amino nitrogen atom interacts with a well-defined water molecule, which sits deep in the active site (Fig. 2*A*). Although the pyrimidine ring is in van der Waals contact with Phe-57, Ile-13, and Leu-45, its *p*-chlorophenyl ring is in contact with the nicotinamide moiety of the NADPH cofactor. Interestingly, the *p*-Cl atom of Pyr lies ≈3.36 Å from the hydroxyl group of Ser-120 with an angle C-Cl···(H)O of 141.8° that can be classified as a H-bond between a weak acceptor and a strong donor, respectively (32, 33). Conformations of Pyr in its unbound and bound states are different such that upon binding to PvDHFR, the angle between the pyrimidine and the phenyl rings of Pyr changes from −116.7° in the free state to −66.3° in the bound form. Because the geometry of the pyrimidine moiety is locked in the binding pocket, the only possible free adjustment is by a simple rotation around a single bond connecting between the two aromatic rings to maximize van der Waals interactions of the *p*-chlorophenyl moiety to the nicotinamide group of the NADPH cofactor.

Enzyme Changes Induced by Mutations. Fig. 2 *A* and *B* shows the structures of the active sites of the PvDHFR from the WT and SP21 mutant, complexed with Pyr. The amino acid residues equivalent to those implicated in substrate catalysis and inhibitor binding of PfDHFR (18, 34) also are found in the active sites of PvDHFR from both sources. The overall structures of WT and mutant enzymes are similar with rmsd fit for all atoms of 0.531 Å. The pyrimidine moiety of the inhibitors is held tightly in the same position in both PvDHFR complexes, whereas the position of the phenyl ring is perturbed by the mutation at codon 117. Nonetheless, distinguishable differences in the orientation of Pyr and NADPH in the active sites of the WT and mutant enzymes can be clearly observed in the binding pocket due to the mutation at Ser-117 → Asn. In the structure of SP21 mutant complexed with Pyr, the Ser-117 → Asn mutation caused steric conflict with the *p*-Cl atom, resulting in displacement of both the *p*-chlorophenyl ring of the inhibitor and a local conformational rearrangement of the peptide chain at residues 118–125, with consequent loss of favorable interactions between the enzyme and the inhibitor. In addition, there was a main-chain movement of α_F (residues 174–178) by 0.3–0.9 Å in the SP21 structure in conjunction with displacement of NADPH. The nicotinamide moiety of the cofactor was both shifted away (0.52 Å) and slightly rotated (dihedral angle of −119.5° to −131.8°) from the optimum position found in the WT enzyme.

Although the conjugated mutation at Ser-58 to Arg did not directly interact with the inhibitor, it might be involved in the substrate (DHF or dihydrofolylpolyglutamate) binding (18).

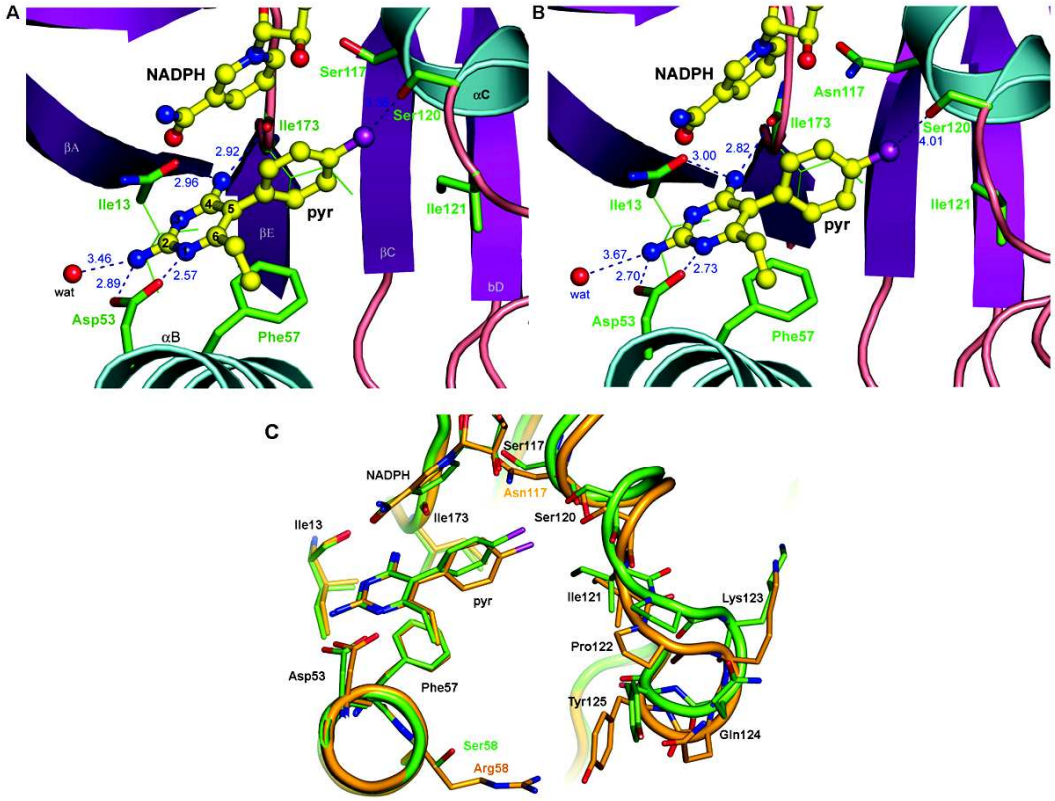

Fig. 2. Pyr bound in the PvDHFR active site. The Pyr and NADPH cofactor are shown as balls and sticks with carbon, nitrogen, and chlorine colored yellow, blue, and magenta, respectively. (*A*) Pyr binding with the WT PvDHFR. Interactions between the enzyme and the pyrimidine ring of the inhibitor include electrostatic interactions and H-bonds indicated by dotted lines. Numbers next to the lines indicate distances in Å. (*B*) Pyr binding with the SP21 double-mutant PvDHFR. Interactions around the pyrimidine ring are similar to the WT enzyme. The mutation at codon 117 from Ser to Asn increases a steric factor in the active site, and, as a result, the positions of both NADPH and Pyr are perturbed from their optimum binding, reducing the efficiency of Pyr by as much as 300-fold. (*C*) Superposition of Pyr-binding sites in the WT PvDHFR (green) and the SP21 double-mutant enzyme (orange) with a rmsd of 0.53 Å. While the position of pyrimidine is held in the same place, the mutation at S117N causes the displacement of *p*-chlorophenyl moiety of Pyr from its optimal binding with the *p*-Cl atom shifted by 1.1 Å and the torsion plane between the two rings twisted by −32°. The mutation also caused a local main-chain movement of residues 118–125 (0.60–1.88 Å), with respect to the WT enzyme. The mutation at codon 58 from Ser to Arg is not in proximity with the Pyr-binding site.

This mutation, located on the α_B helix, from Ser to Arg, created an additional positive charge near the entrance of the active-site cavity but did not perturb the orientation of the helix. In contrast to the equivalent mutation of C59R in PfDHFR-TS structure of which the mutated Arg pointed out into the solvent, the conformation of Arg-58 in the SP21 PvDHFR pointed toward the active-site cavity. Although the position of Arg-58 was too far to interact with the Pyr inhibitor, it in turn interacted with the bound 4-morpholinoethanesulfonate (Mes) molecule used as a crystallization buffer. The Mes molecule was situated in an equivalent position to the α-carboxylic group of the DHF substrate found in the *E. coli* DHFR complex (35), and its binding was mainly favored by salt-bridge interaction between the sulfonate group of Mes and the positive-charged side chain of Arg-131 and Arg-58.

Changes in Inhibitor Binding. Conformational changes of the loop 118–125 are necessary to accommodate Pyr binding in SP21. The dihedral angle of the two aromatic planes of Pyr in the two structures differed by 32° (−66.3° in WT and −98.2° in SP21). The *p*-chlorophenyl ring also was tilted from its original position with the distance difference at the chlorine atom of 1.14 Å. In contrast, a significant displacement is absent in Pyr binding with the equivalent double-mutant K1 PfDHFR (P.C., unpublished results). Moreover, upon accommodation of Pyr, a large conformational change was observed for the SP21–Pyr complex owing to a movement at a peptide region 118–125 by as much as 1.74–1.84 Å for the C^{α} atoms of Pro-122 to Gln-124, ascribed to repulsive interaction between Ile-121 side chain and the *p*-Cl group (Fig. 2*C*). Clearly, the change in the SP21–Pyr complex perilously affects the interaction between the strong H-bond donor hydroxyl side chain of Ser-120 and the weak H-bond acceptor *p*-Cl group of the Pyr with the distance, O(H)···Cl, of 3.36 Å in WT to 4.01 Å in SP21 (32, 33). In addition, the retention of the H-bond (≈3.30 Å) between the side chain of Ser-111 and the *p*-Cl group of Pyr in *P. falciparum* indicates that

BIOCHEMISTRY

Table 2. Inhibition constant (K_i) of recombinant *P. vivax* DHFR with antifolate inhibitors

Inhibitor	K_i, nM		$\Delta(\Delta G°)_{wt\text{-}SP21}$,* kcal·mol^{-1}	$\Delta(\Delta G°)_{Pyr\text{-}Pyr20}$,† kcal·mol^{-1}	
	PvDHFR (WT)	PvDHFR SP21 (S58R+S117N)		WT	SP21
Pyr	0.16 ± 0.03	50 ± 4.0	3.40	1.34	−1.14
Pyr20	1.55 ± 0.12	7.33 ± 0.49	0.92		

*$\Delta(\Delta G°)_{wt\text{-}SP21}$ is the relative binding affinity in comparison of WT–ligand complex with SP21– ligand complex, $-RT\ \ln(K_{i,wt}/K_{i,SP21})$.

†$\Delta(\Delta G°)_{Pyr\text{-}Pyr20}$ is the relative binding affinity of protein in complex with Pyr and Pyr20, $-RT\ \ln(K_{i,pyr}/K_{i,Pyr20})$.

the mutation at Asn-108 in K1 perturbed the inhibitor less than that in *P. vivax*. This structural feature explains why the mutation at Ser-117 causes more reduction in enzyme-binding affinity and a higher level of resistance to Pyr in *P. vivax* than in *P. falciparum*.

The difference in energy caused by loss of the H-bond of Ser-120···*p*-Cl and the loss in van der Waals interaction, together with any entropic penalties paid by the conformational change of the peptide chain at 118–125, resulted in >300-fold loss of Pyr-binding affinity for the double-mutant SP21 PvDHFR, compared with 50- to 90-fold reduction in the K1 PfDHFR-TS (14, 17). The complex of Pyr with the mutant enzyme shows that both Pyr and NADPH are displaced with respect to the WT structure. This displacement of NADPH may contribute to the reduced Pyr-binding affinity, which corresponds to a difference of ≈3.4 kcal·mol^{-1} between mutant and WT enzymes (Table 2) (36, 37).

To clarify the effect of the *p*-Cl moiety of the Pyr, the structures of both WT and SP21 mutant enzymes in complex with Pyr20 were determined (Fig. 3). In WT PvDHFR complexed with Pyr20, the overall structure and the active site were very similar to those of the WT PvDHFR–Pyr complex (rmsd of all C^α atoms = 0.36 Å), and the two inhibitors were in almost identical positions with the dihedral angle between the two rings of −72.3°. However, the binding affinity was reduced by 1.34 kcal·mol^{-1}, presumably equivalent to an internal H-bond in the former complex, apparently due to the lack of the *p*-Cl group on the phenyl substituent of Pyr20 (37).

In the ternary complex structure of SP21 with bound NADPH and Pyr20 (Fig. 3), the steric effect from the mutation of Asn-117 was greatly lessened because of the absence of the *p*-Cl atom in Pyr20. The side chain of Asn-117 readjusted itself to fill up the empty cavity resulting from the missing *p*-Cl atom, such that it interacted with the main-chain carbonyl groups of Ile-173 and Gly-174 as well as H-bonded to the hydroxyl group of Ser-120. Consequently, NADPH returned to its optimal position observed in the WT enzyme. Unlike that of the SP21–Pyr complex, there was neither conformational perturbation of the residues 118–125 nor the NADPH displacement observed in the SP21–Pyr20 complex, substantiating the conclusion that the *p*-Cl group was responsible for the conformational change upon the binding of inhibitor to release the unfavorable contact with the Ile-121 side chain. Nevertheless, the bound Pyr20 was rotated in a similar fashion to the bound Pyr seen in the SP21 mutant, with the dihedral angle of −84.1°, indicating that the larger side chain at codon 117 resulting from the mutation still affects the position of the phenyl ring even without the *p*-Cl atom, and hence the favorable van der Waals interaction has been only partly recovered.

In conclusion, different geometries between Pyr and Pyr20 in the WT and SP21 double mutant of PvDHFRs reflect the effect of the mutations in causing resistance to Pyr and the failure to cause resistance when the Cl atom is removed from the inhibitor. The steric constraint around the side chain of Asn-117 is mainly responsible for the loss of affinity of Pyr for PvDHFR, with consequent displacement of both the inhibitor and NADPH, and conformational changes to optimize binding. The detailed structural results we report for drug complexes of the WT and SP21-resistant strain of PvDHFR support a compelling explanation for the mechanism of molecular resistance.

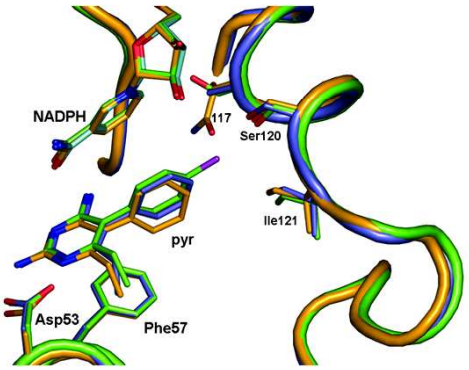

Fig. 3. Superposition of the Pyr binding-site of WT PvDHFR–Pyr20 (dechloropyrimethamine) complex (cyan) and SP21 PvDHFR–Pyr20 complex (orange) onto of the WT PvDHFR–Pyr complex (green). The steric hindrance of Asn-117 is lessened in the case of Pyr20-bound enzymes with neither movement of the nicotinamide moiety nor the local changes in residues 118–125 but only slight displacement of phenyl ring. Pyr20 binds with the WT enzyme similar to Pyr. Pyr, Pyr20, and NADPH are depicted as stick models.

Implications for the Molecular Mechanism of Resistance. Our observation leads to some important conclusion for the mechanism of resistance of *P. vivax* to antifolate drugs. First, because our results show that Pyr binds well with the WT PvDHFR, the WT parasite is likely sensitive to the drug and only becomes resistant on mutations that disturb drug binding, supporting earlier observations (10, 38, 39). Second, the poorer binding of Pyr to SP21 PvDHFR is caused by steric clash between Ser-117 → Asn and the *p*-Cl atom, whereas the Pyr20 (which fits approximately within the substrate envelope) binds relatively well to both WT (1.5 nM) and SP21 mutant enzyme (7 nM). Resistance therefore was generated through mutations that can occur to disrupt binding with the parts of the inhibitor that protrude beyond the envelope of the substrate. This general idea of developing resistance-avoiding inhibitors also is supported by our previous work on the Pf-DHFRTS–WR99210 complex (34), which showed that this flexible inhibitor binds well to both WT and Pyr-resistant strains by adopting a conformation that keeps it within the substrate envelope. A similar picture has been shown for resistance to HIV protease inhibitor drugs (40, 41). Structural studies in HIV protease show that the small flexible nature of the inhibitor such as tenofovir enables it to stay in the small substrate envelope and avoid the surveillance mechanism used by reverse-transcriptase inhibitor-resistance mutants, whereas

those inhibitors protruding beyond the substrate envelope can develop mutations in the active site that confer resistance.

These structural results point the way to the design of new generations of antimalarial antifolate drugs in which the basic structural rules for avoiding resistance are now postulated. One approach is to design inhibitors that stay approximately within the substrate space of the DHFR, such as Pyr20 (39, 42). However, because these inhibitors may still induce further resistance as shown in ref. 15, additional approaches, such as employing combination of inhibitors that require different sets of mutations to generate resistance as has been noted for Pyr and WR99210 (39, 42), are needed.

This work was supported by the Thailand Research Fund and the Thailand-Tropical Diseases Research Program (P. Kongsaeree), the Wellcome Trust (Y.Y. and M.D.W.), and the Medicines for Malaria Venture and European Union International Cooperation–Developing Countries (INCO-Dev) (Y.Y.). P. Khongsuk was supported by scholarships from the Postgraduate Education and Research Program in Chemistry and National Centre for Genetic Engineering and Biotechnology (Thailand).

1. Sina, B. (2002) *Trends Parasitol.* **18,** 287–289.
2. Mendis, K., Sina, B. J., Marchesini, P. & Carter, R. (2001) *Am. J. Trop. Med. Hyg.* **64,** 97–106.
3. Schwartz, I. K., Lackritz, E. M. & Patchen, L. C. (1991) *New Engl. J. Med.* **324,** 927.
4. Rieckmann, K. H., Davis, D. R. & Hutton, D. C. (1989) *Lancet* **2,** 1183–1184.
5. Kublin, J. G., Cortese, J. F., Njunju, E. M., Mukadam, R. A., Wirima, J. J., Kazembe, P. N., Djimde, A. A., Kouriba, B., Taylor, T. E. & Plowe, C. V. (2003) *J. Infect. Dis.* **187,** 1870–1875.
6. Hastings, I. M., Bray, P. G. & Ward, S. A. (2002) *Science* **298,** 74–75.
7. Peters, W. (1998) *Adv. Parasitol.* **41,** 1–62.
8. de Pecoulas, P. E., Tahar, R., Ouatas, T., Mazabraud, A. & Basco, L. K. (1998) *Mol. Biochem. Parasitol.* **92,** 265–273.
9. Imwong, M., Pukrittakayamee, S., Looareesuwan, S., Pasvol, G., Poirreiz, J., White, N. J. & Snounou, G. (2001) *Antimicrob. Agents Chemother.* **45,** 3122–3127.
10. Leartsakulpanich, U., Imwong, M., Pukrittayakamee, S., White, N. J., Snounou, G., Sirawaraporn, W. & Yuthavong, Y. (2002) *Mol. Biochem. Parasitol.* **119,** 63–73.
11. Eldin de Pecoulas, P., Basco, L. K., Tahar, R., Ouatas, T. & Mazabraud, A. (1998) *Gene* **211,** 177–185.
12. Yuthavong, Y. (2002) *Microbes Infect.* **4,** 175–182.
13. Warhurst, D. C. (2002) *Sci. Prog.* **85,** 89–111.
14. Sirawaraporn, W., Sathitkul, T., Sirawaraporn, R., Yuthavong, Y. & Santi, D. V. (1997) *Proc. Natl. Acad. Sci. USA* **94,** 1124–1129.
15. Chusacultanachai, S., Thiensathit, P., Tarnchompoo, B., Sirawaraporn, W. & Yuthavong, Y. (2002) *Mol. Biochem. Parasitol.* **120,** 61–72.
16. Sirawaraporn, W., Yongkiettrakul, S., Sirawaraporn, R., Yuthavong, Y. & Santi, D. V. (1997) *Exp. Parasitol.* **87,** 245–252.
17. Tarnchompoo, B., Sirichaiwat, C., Phupong, W., Intaraudom, C., Sirawaraporn, W., Kamchonwongpaisan, S., Vanichtanankul, J., Thebtaranonth, Y. & Yuthavong, Y. (2002) *J. Med. Chem.* **45,** 1244–1252.
18. Yuvaniyama, J., Chitnumsub, P., Kamchonwongpaisan, S., Vanichtanankul, J., Sirawaraporn, W., Taylor, P., Walkinshaw, M. D. & Yuthavong, Y. (2003) *Nat. Struct. Biol.* **10,** 357–365.
19. Sardarian, A., Douglas, K. T., Read, M., Sims, P. F., Hyde, J. E., Chitnumsub, P., Sirawaraporn, R. & Sirawaraporn, W. (2003) *Org. Biomol. Chem.* **1,** 960–964.
20. Rastelli, G., Sirawaraporn, W., Sompornpisut, P., Vilaivan, T., Kamchonwongpaisan, S., Quarrell, R., Lowe, G., Thebtaranonth, Y. & Yuthavong, Y. (2000) *Bioorg. Med. Chem.* **8,** 1117–1128.
21. D'Arcy, A., Elmore, C., Stihle, M. & Johnston, J. E. (1996) *J. Cryst. Growth* **168,** 175–180.
22. Pflugrath, J. W. (1999) *Acta Crystallogr. D* **55,** 1718–1725.
23. Navaza, J. (2001) *Acta Crystallogr. D* **57,** 1367–1372.
24. McRee, D. E. (1999) *J. Struct. Biol.* **125,** 156–165.
25. Brunger, A. T., Adams, P. D., Clore, G. M., DeLano, W. L., Gros, P., Grosse-Kunstleve, R. W., Jiang, J. S., Kuszewski, J., Nilges, M., Pannu, N. S., *et al.* (1998) *Acta Crystallogr. D* **54,** 905–921.
26. Engh, R. A. & Huber, R. (1991) *Acta Crystallogr. A* **47,** 392–400.
27. Laskowski, R. A. (1993) *J. Appl. Crystallogr.* **26,** 283.
28. Westhead, D. R., Slidel, T. W., Flores, T. P. & Thornton, J. M. (1999) *Protein Sci.* **8,** 897–904.
29. Matthews, D. A., Alden, R. A., Bolin, J. T., Freer, S. T., Hamlin, R., Xuong, N., Kraut, J., Poe, M., Williams, M. & Hoogsteen, K. (1977) *Science* **197,** 452–455.
30. Rastelli, G., Pacchioni, S. & Parenti, M. D. (2003) *Bioorg. Med. Chem. Lett.* **13,** 3257–3260.
31. Zhang, K. & Rathod, P. K. (2002) *Science* **296,** 545–547.
32. Aullon, G., Bellamy, D., Orpen, G. A., Brammer, L. & Bruton, E. A. (1998) *Chem. Commun.*, 653–654.
33. Brammer, L., Bruton, E. A. & Sherwood, P. (2001) *Cryst. Growth Des.* **1,** 277–290.
34. Yuthavong, Y., Yuvaniyama, J., Chitnumsub, P., Vanichtanankul, J., Chusacultanachai, S., Tarnchompoo, B., Vilaivan, T. & Kamchonwongpaisan, S. (2005) *Parasitology* **130,** 249–259.
35. Sawaya, M. R. & Kraut, J. (1997) *Biochemistry.* **36,** 586–603.
36. Meyer, E. A., Castellano, R. K. & Diederich, F. (2003) *Angew. Chem. Int. Ed.* **42,** 1210–1250.
37. Myers, J. K. & Pace, C. N. (1996) *Biophys. J.* **71,** 2033–2039.
38. Tahar, R., de Pecoulas, P. E., Basco, L. K., Chiadmi, M. & Mazabraud, A. (2001) *Mol. Biochem. Parasitol.* **113,** 241–249.
39. Hastings, M. D. & Sibley, C. H. (2002) *Proc. Natl. Acad. Sci. USA* **99,** 13137–13141.
40. Larder, B. (2001) *AIDS* **15,** S27–S34.
41. King, N. M., Prabu-Jeyabalan, M., Nalivaika, E. A. & Schiffer, C. A. (2004) *Chem. Biol.* **11,** 1333–1338.
42. Ridley, R. G. (2002) *Proc. Natl. Acad. Sci. USA* **99,** 13362–13364.